International Journal of Solids and Structures 50 (2013) 447–455

Contents lists available at SciVerse ScienceDirect

International Journal of Solids and Structures

journal homepage: www.elsevier.com/locate/ijsolstr

Extension of a shear-controlled ductile fracture model considering the stress triaxiality and the Lode parameter

Yanshan Lou, Hoon Huh *

School of Mechanical, Aerospace and Systems Engineering, KAIST, 335, Gwahangno, Daeduk Science Town, Daejeon 305-701, South Korea

ARTICLE INFO

Article history:
Received 18 April 2012
Received in revised form 5 July 2012
Available online 23 October 2012

Keywords:
Ductile fracture criterion
Fracture locus
Mohr–Coulomb criterion
Bulk metal forming

ABSTRACT

This paper is concerned with the extension of a shear-controlled ductile fracture criterion for accurate prediction of fracture forming limit diagrams (FFLD) in sheet metal forming processes. A shear-controlled ductile fracture criterion is extended to a general three-dimensional stress space with dependence on the stress triaxiality and the Lode parameter. The underlying mechanisms of Lode parameter dependence of ductile fracture are first correlated to the effect of the maximum shear stress on shear-coalescence of voids. The effect of the stress triaxiality and the Lode parameter on the equivalent plastic strain to fracture is investigated in the space of $(\eta, L, \bar{\varepsilon})$. For the purpose of comparison, the Mohr–Coulomb criterion is also transformed into the space of $(\eta, L, \bar{\varepsilon})$ using the technique of the Mohr's circles. Both criteria are applied to construct fracture loci of Al 2024-T351. Fracture loci constructed are compared to experimental data points to validate the performance of two criteria. The comparison demonstrates that fracture loci constructed by two criteria are close to experimental results except for two data points in the high stress triaxiality. The big difference between two criteria is that a cut-off value for the stress triaxiality is extremely small for the Mohr–Coulomb criterion while the new ductile fracture criterion endows a constant cut-off value of $-1/3$ which is reasonable for ductile materials. Due to this limitation of the Mohr–Coulomb criterion, the new criterion is more suitable to model ductile fracture in metal forming processes.

1. Introduction

Two types of failure models are dominant in metal forming: necking and ductile fracture. Necking failure takes place in tension while ductile fracture is observed not only in tension but also in shear and compression such as tube torsion and compressive upsetting tests. For sheet metals, necking is widely accepted as the main failure model from the uniaxial tension to the balanced biaxial tension. Many analytical necking models (Hill, 1952; Hora et al., 1996; Marciniak and Kuczynski, 1967; Stören and Rice, 1975; Swift, 1952; Zhu et al., 2001) were proposed based on different assumptions to predict the forming limit of sheet metals. The forming limit predicted by necking models are generally plotted in the space of $(\varepsilon_1, \varepsilon_2)$ and named as forming limit diagrams (FLDs), which was first proposed by Keeler and Backofen (1963) and Goodwin (1968). Necking models, however, cannot estimate the forming limit in shear and compression conditions since thickness reduction is negligible in shear or thickening is observed in compression.

Ductile fracture criteria are alternative and powerful choices to predict the onset of fracture for metals and alloys. The essential merit of ductile fracture criteria is that they can predict the failure of materials in shear and compression with the low and negative stress triaxiality. Ductile fracture criteria are blessed with this capability due to the fact that their primitive basis is damage accumulation caused by nucleation, growth and coalescence of microscopic voids instead of necking or thinning.

Mechanisms of nucleation, growth and coalescence of voids were extensively investigated and analyzed experimentally, theoretically and numerically (Argon et al., 1975; Goods and Brown, 1979; Gurson, 1977; McClintock, 1968; Rice and Tracey, 1969; Weck and Wilkinson, 2008). Based on various analytical and numerical studies as well as experimental observation, dozens of coupled and uncoupled ductile fracture criteria (Brozzo et al., 1972; Clift et al., 1990; Cockcroft and Latham, 1968; Gurson, 1977; LeRoy et al., 1981; Ko et al., 2007; Nielsen and Tvergaard, 2010; Oh et al., 1979; Oyane et al., 1980; Rice and Tracey, 1969; Tvergaard and Needleman, 1984; Xue, 2007, 2008; Xue and Wierzbicki, 2008) were proposed with various hypotheses.

The Mohr–Coulomb criterion, extensively and originally used in rock and soil and other relatively brittle materials, was successfully transformed to construct the fracture locus in the space of $(\eta, \bar{\theta}, \bar{\varepsilon})$ by combining the Mohr–Coulomb criterion with a new hardening rule with pressure and Lode angle dependence (Bai and Wierzbicki, 2010). Li et al. (2010) applied the modified Mohr–Coulomb (MMC) criterion to predict shear-induced fracture in sheet metal forming. Failure in stretch-bending tests is accurately predicted by the MMC

* Corresponding author. Tel.: +82 42 350 3222; fax: +82 42 350 3210.
E-mail address: hhuh@kaist.ac.kr (H. Huh).

0020-7683/$ - see front matter © 2012 Elsevier Ltd. All rights reserved.
http://dx.doi.org/10.1016/j.ijsolstr.2012.10.007

Nomenclature

$\varepsilon_1, \varepsilon_2$	principal strains in the plane stress conditions, $\varepsilon_1 \geqslant \varepsilon_2$
$\varepsilon_I, \varepsilon_{II}, \varepsilon_{III}$	orderless principal strains in full stress states
$\bar{\varepsilon}, \bar{\varepsilon}_f$	equivalent plastic strain and equivalent plastic strain to fracture
$\sigma_1, \sigma_2, \sigma_3$	principal stresses, $\sigma_1 \geqslant \sigma_2 \geqslant \sigma_3$
s_1, s_2, s_3	deviatoric principal stresses, $s_1 \geqslant s_2 \geqslant s_3$
σ_m	mean or hydrostatic stress, $\sigma_m = (\sigma_1 + \sigma_2 + \sigma_3)/3$
$\bar{\sigma}$ or σ_e	von Mises equivalent stress
σ, τ	normal stress and shear stress in the Mohr–Coulomb criterion
τ_{max}	maximum shear stress
η	stress triaxiality, $\eta = \sigma_m/\bar{\sigma}$
$L, \theta, \bar{\theta}$	Lode parameter, Lode angle and Lode angle parameter
K, ε_0, n	coefficients in the Swift hardening model
C_1, C_2, C_3	material constants in the new ductile fracture criterion
c, ϕ	material constants in the Mohr–Coulomb criterion
γ	parameter in two Lode dependent functions

criterion (Chen et al., 2010; Luo et al., 2010). The MMC criterion, however, predict an extremely low cut-off value for the stress triaxiality where fracture will never occur for ductile materials (Bai and Wierzbicki, 2010). The extremely small cut-off value for the stress triaxiality predicted by the MMC criterion is sound for brittle materials but conflicts with experimental observation of upsetting tests for ductile materials (Bridgman, 1964). Lou et al. (2012) proposed a simple uncoupled ductile fracture criterion to describe fracture behavior of sheet metals for nucleation, growth and shear coalescence of voids. The essential merit of this criterion is that a constant cut-off value of $-1/3$ for the stress triaxiality is intentionally endowed for sheet metals as presented in Fig. 1 for Al 2024-T351.

In this paper, a new ductile fracture criterion (Lou et al., 2012) as well as the Mohr–Coulomb criterion is transformed into the general three-dimensional stress state in the space of $(\eta, L, \bar{\varepsilon})$. Both criteria are applied to construct fracture loci of Al 2024-T351 (Bai and Wierzbicki, 2010). The fracture loci constructed are compared with experimental data points to validate their performance on prediction of the equivalent plastic strain to fracture for bulk metals.

2. Extension of a new ductile fracture criterion

2.1. Review of a newly proposed ductile fracture criterion

A new ductile fracture criterion (Lou et al., 2012) was developed with consideration of damage accumulation induced by nucleation, growth and shear coalescence of voids, which has a form of

$$\left(\frac{2\tau_{max}}{\bar{\sigma}}\right)^{C_1}\left(\frac{\langle 1+3\eta\rangle}{2}\right)^{C_2}\bar{\varepsilon}_f = C_3 \quad \langle x\rangle = \begin{cases} x & \text{when} \quad x \geqslant 0 \\ 0 & \text{when} \quad x < 0 \end{cases} \tag{1}$$

In this new ductile fracture criterion, the void nucleation was assumed to be proportional to the equivalent plastic strain $\bar{\varepsilon}$, the void growth was represented as a function of the stress triaxiality as $1 + 3\eta$, and shear coalescence of voids was described by the normalized maximum shear stress $\tau_{max}/\bar{\sigma}$. Two material constants C_1 and C_2 were introduced as exponents to both the normalized maximum shear stress term and the stress triaxiality term to modulate different effects of nucleation, growth and coalescence of voids on ductile fracture. A constant cut-off value of $-1/3$ was intentionally endowed for the stress triaxiality (Lou et al., 2012). Recently, Khan and Liu (2012) observed ductile fracture biaxial compressive loading conditions with a stress triaxiality below $-1/3$, which the new ductile fracture criterion was successfully applied to predict the fracture locus of Al 2024-T351 in the plane stress condition as presented in Fig. 1. When the loading path and the deformation path are not proportional, Eq. (1) can be restated to trace non-proportional or non-linear path of deformation as below:

$$\frac{1}{C_3}\int_0^{\bar{\varepsilon}_f}\left(\frac{2\tau_{max}}{\bar{\sigma}}\right)^{C_1}\left(\frac{\langle 1+3\eta\rangle}{2}\right)^{C_2} d\bar{\varepsilon} = D(\bar{\varepsilon})$$
$$\langle x\rangle = \begin{cases} x & \text{when} \quad x \geqslant 0 \\ 0 & \text{when} \quad x < 0 \end{cases} \tag{2}$$

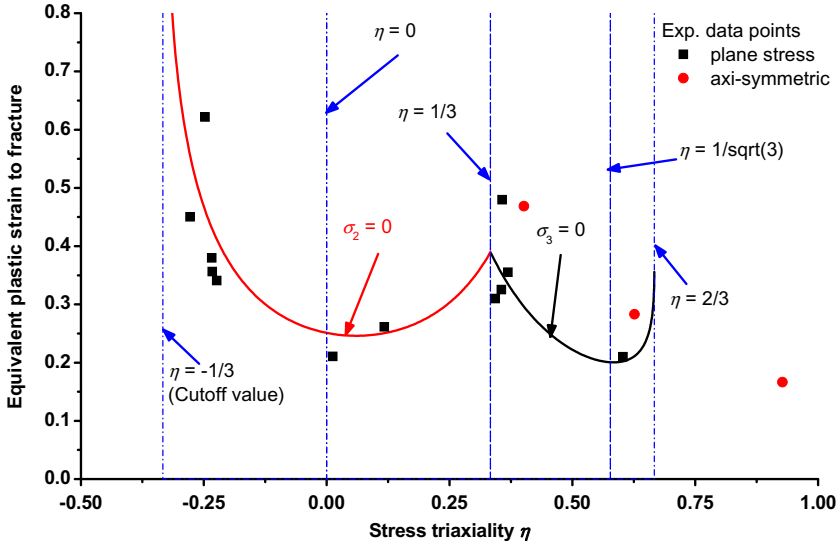

Fig. 1. Comparison of the fracture locus constructed by a new criterion of Eq. (1) to experimental data points of Al2024-T351 in the space of $(\eta, \bar{\varepsilon}\bar{\varepsilon})$. Lou et al. (2012).

The integral form of the new criterion in Eq. (2) can be utilized in complicated non-linear simulation of sheet metal forming, which is path dependent.

Recently, Khan and Liu (2012) observed ductile fracture in biaxial compressive loading conditions with a stress triaxiality below −1/3, which indicates the limitation of the reports from Bao and Wierzbicki (2005). Aretz (2011) stated that the cut-off value is different for different materials because different materials have different microstructures and thus different sensitivities to damage under compressive loading and also thought that it is quite natural that the cut-off value should be different for different Lode parameters in case that the Lode parameter and the stress triaxialtiy are independent variables. In addition, the cut-off value for the stress triaxiality is expected to rise with testing temperature since metals become ductile as temperature increases and high temperature improves their ductility such as hot forming of advanced high strength steel, aluminum alloys and warm forming of magnesium alloys. In order to meet such variations, the ductile fracture criterion needs to be modified to consider a changeable cut-off value for the stress triaxiality as below:

$$\left(\frac{2\tau_{\max}}{\bar{\sigma}}\right)^{C_1}\left(\left\langle\frac{f(\eta,L)}{f(1/3,-1)}\right\rangle\right)^{C_2}\bar{\varepsilon}_f = C_3 \quad \langle x\rangle = \begin{cases} x & \text{when } x \geqslant 0 \\ 0 & \text{when } x < 0 \end{cases} \tag{3}$$

where $f(\eta, L)$ is the Lode dependent cut-off value for the stress triaxiality which is changeable according to microstructures of metals and temperature and $f(1/3, -1)$ indicates the uniaxial tensile condition. The modified model of Eq. (3) reduces to the original form in Eq. (1) when $f(\eta, L) = 1 + 3\eta$.

However, it is still a great challenge to accurately determine the exact value for the stress triaxiality as well as effect of the Lode parameter on the cut-off value for the stress triaxiality based on current experimental techniques. Thus, the cut-off value of −1/3 reported by Bao and Wierzbicki (2005) was still adopted in the current model and used in this paper.

2.2. Transformation between $(\sigma_1, \sigma_2, \sigma_3)$ and $(\eta, L, \bar{\sigma})$

To extend the new ductile fracture criterion in Eq. (1) with dependence on the stress triaxiality and the Lode parameter, the transformation between $(\sigma_1, \sigma_2, \sigma_3)$ and $(\eta, L, \bar{\sigma})$ should be first derived. If the stress state is expressed as $(\sigma_1, \sigma_2, \sigma_3)$ in the principal stress space, the stress triaxiality and the Lode parameter are calculated by their definitions as follows (Fung and Tong, 2001; Lode, 1926):

$$\eta = \frac{\sigma_m}{\bar{\sigma}} = \frac{\sigma_1 + \sigma_2 + \sigma_3}{3\bar{\sigma}} \tag{4}$$

$$L = \frac{2\sigma_2 - \sigma_1 - \sigma_3}{\sigma_1 - \sigma_3} \tag{5}$$

From Eqs. (4) and (5) as well as the von Mises yield function, the stress state is easily transformed from $(\sigma_1, \sigma_2, \sigma_3)$ to $(\eta, L, \bar{\sigma})$. The transformation will be then derived from $(\eta, L, \bar{\sigma})$ to $(\sigma_1, \sigma_2, \sigma_3)$. From Eq. (5) and the von Mises yield function, the following relation is obtained:

$$\frac{\sigma_1 - \sigma_3}{2} = \frac{\bar{\sigma}}{\sqrt{L^2+3}} \tag{6}$$

From the definition of η and L as well as Eq. (6), the following equation is derived:

$$\frac{\sigma_1 + \sigma_3}{2} = \sigma_m - \frac{\bar{\sigma}L}{3\sqrt{L^2+3}} = \left(\eta - \frac{L}{3\sqrt{L^2+3}}\right)\bar{\sigma} \tag{7}$$

From Eqs. (6) and (7) as well as Eqs. (4) and (5), the stress state is successfully transformed from $(\eta, L, \bar{\sigma})$ to $(\sigma_1, \sigma_2, \sigma_3)$ as follows:

$$\sigma_1 = \sigma_m + s_1 = \sigma_m + \frac{(3-L)\bar{\sigma}}{3\sqrt{L^2+3}} = \left(\eta + \frac{(3-L)}{3\sqrt{L^2+3}}\right)\bar{\sigma} \tag{8}$$

$$\sigma_2 = \sigma_m + s_2 = \sigma_m + \frac{2L\bar{\sigma}}{3\sqrt{L^2+3}} = \left(\eta + \frac{2L}{3\sqrt{L^2+3}}\right)\bar{\sigma} \tag{9}$$

$$\sigma_3 = \sigma_m + s_3 = \sigma_m - \frac{(3+L)\bar{\sigma}}{3\sqrt{L^2+3}} = \left(\eta - \frac{(3+L)}{3\sqrt{L^2+3}}\right)\bar{\sigma} \tag{10}$$

2.3. Extension to the space of $(\eta, L, \bar{\varepsilon})$

Since transformation of the stress state between $(\sigma_1, \sigma_2, \sigma_3)$ and $(\eta, L, \bar{\sigma})$ is derived above, the extension of the new ductile fracture criterion of Eq. (1) to the general three-dimensional space is quite simple. The maximum shear stress is a half of the difference between the maximum and minimum principal stresses denoting $\tau_{\max} = (\sigma_1 - \sigma_3)/2$. Putting this relation into Eq. (6) generates the equation below:

$$\frac{2\tau_{\max}}{\bar{\sigma}} = \frac{2}{\sqrt{L^2+3}} \tag{11}$$

The new ductile fracture criterion of Eq. (1) is transformed into the space of $(\eta, L, \bar{\varepsilon})$ by replacing the normalized maximum shear stress as a function of L in Eq. (11) as below:

$$\left(\frac{2}{\sqrt{L^2+3}}\right)^{C_1}\left(\frac{\langle 1+3\eta\rangle}{2}\right)^{C_2}\bar{\varepsilon}_f = C_3 \quad \langle x\rangle = \begin{cases} x & \text{when } x \geqslant 0 \\ 0 & \text{when } x < 0 \end{cases} \tag{12}$$

Since three material constants C_1, C_2 and C_3 are positive. The equivalent plastic strain to fracture monotonically decreases with the stress triaxiality since a high stress triaxiality accelerates void growth thereby reducing ductility. The equivalent plastic strain to fracture is symmetric with respect to $L = 0$ because the normalized maximum shear stress is also a symmetric function of the Lode parameter L as presented in Eq. (11). For the application to numerical analyses, the integral form of the ductile fracture criterion of Eq. (12) needs to be expressed as below:

$$\frac{1}{C_3}\int_0^{\bar{\varepsilon}_f}\left(\frac{2}{\sqrt{L^2+3}}\right)^{C_1}\left(\frac{\langle 1+3\eta\rangle}{2}\right)^{C_2} d\bar{\varepsilon} = D(\bar{\varepsilon}) \quad \langle x\rangle = \begin{cases} x & \text{when } x \geqslant 0 \\ 0 & \text{when } x < 0 \end{cases} \tag{13}$$

Fracture initiates when the accumulated damage $D(\bar{\varepsilon})$ reaches to unity.

2.4. Lode parameter dependence analysis

Both experimental (Bridgman, 1964; Kao et al., 1990) and analytical studies (McClintock, 1968; Rice and Tracey, 1969) demonstrated that the fracture strain reduces as the stress triaxiality increases. Concerning the dependence on the stress triaxiality, it can be easily concluded that the equivalent plastic strain to fracture in the uniaxial tension ($\eta = 1/3$) is less than that in the pure shear ($\eta = 0$) due to the lack of the stress triaxiality for the growth of voids in the pure shear. This conclusion, however, conflicts with some experimental results which showed that the equivalent plastic strain to fracture in the pure shear was lower than that in the uniaxial tension for Al 2024-T351 (Bao and Wierzbicki, 2004), 1045 steel (Bridgman, 1964) and 4340 steel (Halford and Morrow, 1962). This conflict was attributed to the overlook of the Lode angle dependence in ductile fracture (Xue, 2007, 2008; Xue and Wierzbicki, 2008). Xue (2007) and Xue and Wierzbicki (2008) proposed

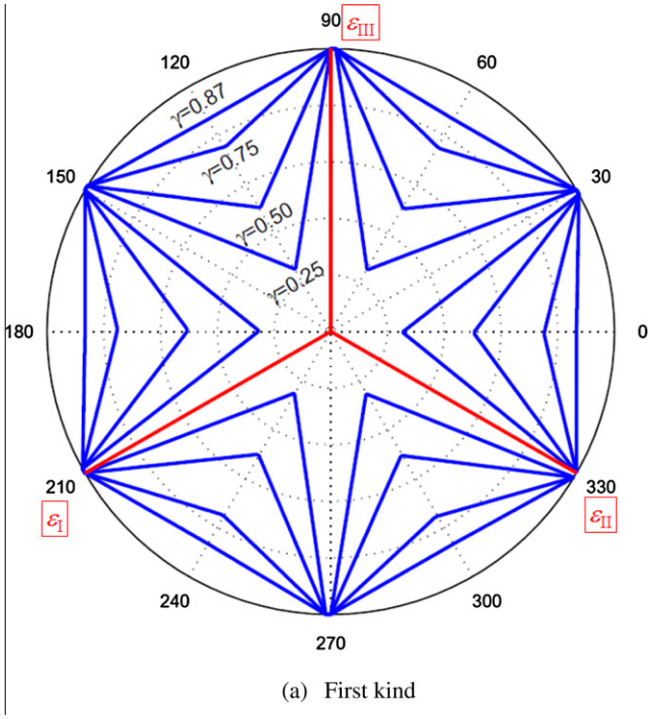

(a) First kind

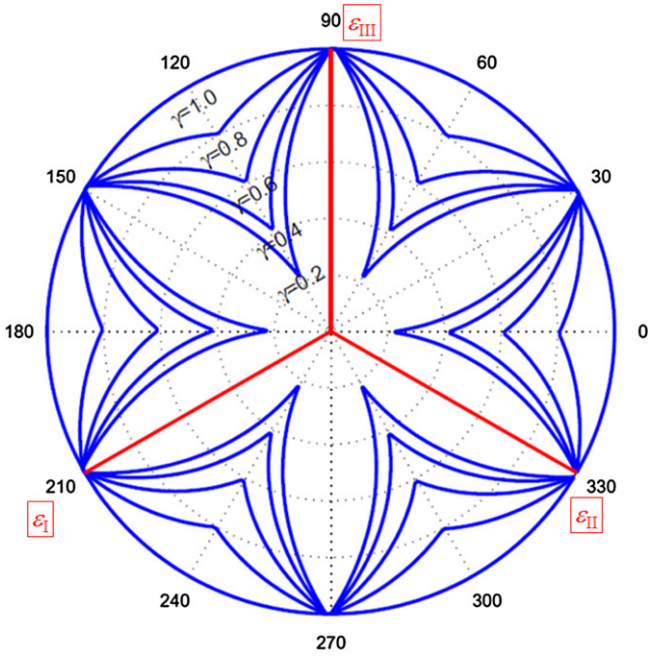

(b) Second kind

Fig. 2. Two kinds of Lode dependence functions: (a) first kind; (b) second kind. Xue (2007).

two Lode angle dependence models in a heuristic way since there was so far no conclusive experimental results to show the shape of the Lode angle dependence function due to the fact that experimental apparatuses have not been set up to test material properties under a constant hydrostatic pressure. These two Lode angle dependence functions are graphically illustrated in Fig. 2 referred from Xue (2007) and Xue and Wierzbicki (2008), although its physical mechanism remained ambiguous (Li et al., 2009).

The proposed ductile fracture criterion in Eq. (1) motivated by the microscopic and experimental observations does not incorporate the Lode angle dependence in ductile fracture explicitly. The Lode angle dependence, however, is obviously incorporated in the transformed form in Eq. (12) since the Lode angle and the Lode angle parameter have a one-to-one relation with the Lode parameter as presented in Eqs. (24) and (25) in Section 5.1. The transformation processes indicate that the Lode parameter dependence is implicitly coupled with the assumption that the coalescence of voids is controlled by the maximum shear stress. The assumption of shear-controlled void coalescence provides a reasonable explanation for the mechanism of the Lode parameter dependence in ductile fracture since a high shear stress facilitates the coalescence of voids and reduces the equivalent plastic strain to fracture. As shown in Fig. 3 of Eq. (11), the normalized maximum shear stress is a concave function of the Lode parameter and symmetric with respect to $L = 0$. The normalized maximum shear stress at $L = 0$ well resolves the above conflict between experimental observation and fracture criteria ignoring the Lode parameter dependence. Moreover, experiments also demonstrated a higher fracture strain in the pure shear than that in the uniaxial tension for rolled 60–40 brass, 1100-O aluminum annealed 660 °F and 7075-T6 aluminum alloy (Halford and Morrow, 1962) as well as TRIP780 steel sheet (Dunand and Mohr, 2011), which indicates variation of Lode parameter sensitivity for different materials. This variation of Lode parameter sensitivity is properly coupled in the new ductile fracture criterion with different values of C_1 as represented in Fig. 4. When $C_1 = 0$, the Lode dependence of ductile fracture vanishes and the fracture locus at a constant stress triaxiality degenerates to a perfect circle. A right hexagonal fracture locus is formed when $C_1 = 1$. A six-point star is constructed when $C_1 > 1$. Discontinuity is observed at six vertices of $L = \pm 1$ since the direction of the fracture surface change due to the change of the maximum shear stress direction. Compared with two Lode parameter dependence functions in Fig. 2, a smooth fracture locus in six valleys at $L = 0$ is the characteristics of the Lode parameter dependence function in the new ductile fracture criterion. The smoothness of the fracture locus at $L = 0$ is quite natural since there is no direction change of the fracture surface and the maximum shear stress between both sides of $L = 0$. Moreover, it should be noted that the six vertices at $L = \pm 1$ cannot be easily achieved in experiments since ductile fracture is inclined in the shortest way to take place in the valley in the shear mode. This tendency was also proved by the Marciniak and Kuczynski (1967) model *in which the strain path in the imperfect groove approaches the plane strain condition* ($L = 0$) *even though the strain path outside the groove is still linear.*

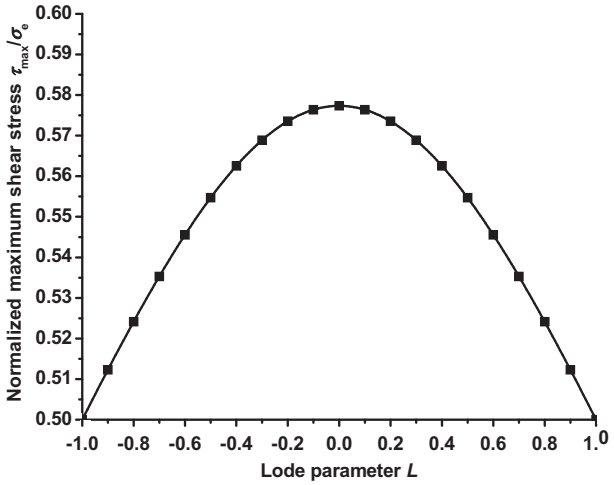

Fig. 3. Lode dependence of the normalized maximum shear stress in Eq. (11).

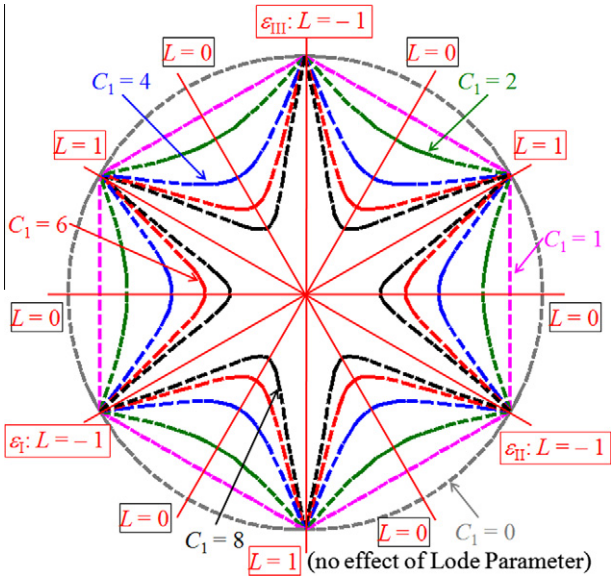

Fig. 4. Lode dependence of the new ductile fracture criterion. ($C_2 = 0.2235$, $C_3 = 0.3896$, $\eta = 0$).

3. Parameter study

There are three material constants in the new ductile fracture criterion. Lou et al. (2012) investigated effects of material constants on FFLDs in the space of $(\varepsilon_2, \varepsilon_1)$ for sheet metals. Their effects will be analyzed in the space of $(\eta, L, \bar{\varepsilon})$ for the generalized three-dimensional stress states in the following sections.

3.1. Effect of the material constant C_1

The effect of the normalized maximum shear stress on shear coalescence of voids is modulated by the material constant C_1 as presented in Eq. (1). High normalized maximum shear stress reduced the equivalent plastic strain to fracture. The fracture locus is constructed with different values of C_1 in Fig. 5. The curvature of the constructed fracture locus is observed to rise with C_1. When C_1 increases, the equivalent plastic strain to fracture remains constant at $L = \pm 1$ but decreases in between.

3.2. Effect of the material constant C_2

The material constant C_2 modulates the effect of the stress triaxiality on void growth. As C_2 increases, the influence of the stress triaxiality is magnified on the equivalent plastic strain to fracture. Its effect is graphically illustrated in Fig. 6. The equivalent plastic strain to fracture decreases as the stress triaxiality increases, which makes sense considering damage accumulation induced by void growth. The constructed fracture locus somewhat rotates around the interacting line at $\eta = 1/3$ with different values of C_2.

3.3. Effect of the material constant C_3

The material constant C_3 is equal to the equivalent plastic strain to fracture in the uniaxial tension with $\eta = -1/3$ and $L = -1$. C_3 modulates the magnitude of the constructed fracture locus with no influence on the shape of constructed fracture locus as presented in Fig. 7.

4. The Mohr–Coulomb criterion

The Mohr–Coulomb criterion, which has been successfully and widely used in the relative brittle materials such as rock and soil,

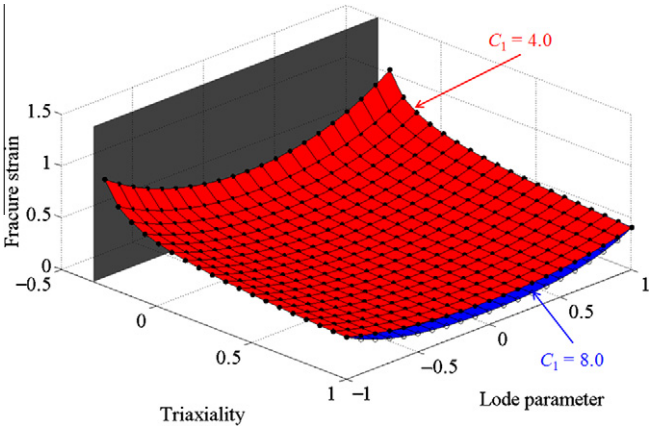

Fig. 5. Effect of the material constant C_1 in spaces of $(\eta, L, \bar{\varepsilon})$. ($C_2 = 0.3$, $C_3 = 0.5$).

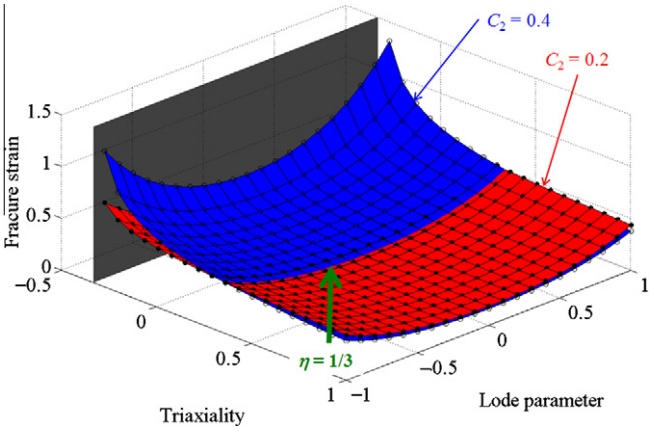

Fig. 6. Effect of the material constant C_2 in spaces of $(\eta, L, \bar{\varepsilon})$. ($C_1 = 6.0$, $C_3 = 0.5$).

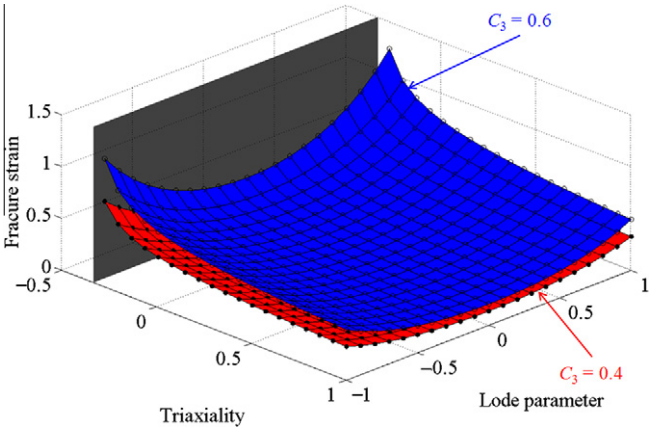

Fig. 7. Effect of the material constant C_3 in spaces of $(\eta, L, \bar{\varepsilon})$. ($C_1 = 6.0$, $C_2 = 0.3$).

attracted increasing concerns of scientists and researchers who studied ductile fracture of metals in the last several years. Wierzbicki et al. (2005) showed that the Tresca criterion, a special case of the Mohr–Coulomb criterion, was the most faithful failure condition with the greatest robustness among seven ductile fracture criteria. Bai and Wierzbicki (2010) analyzed and transformed the Mohr–Coulomb criterion to the space of $(\eta, \bar{\theta}, \bar{\varepsilon})$ by solving a complicated maximum value problem using a Lagrangian multiplier technique. In the following section, the Mohr–Coulomb criterion

is first analyzed with a more efficient procedure than the original one using the technique of the Mohr's circles.

The Mohr–Coulomb criterion postulates that fracture takes place in a body on a plane on which the combination of the normal and shear stresses reaches a critical value. A special case of the Mohr–Coulomb criterion is that the normal and shear stresses are linearly combined as below:

$$\tau + \sigma \tan\phi = c \tag{14}$$

where c is a material constant and ϕ is the angle of internal friction as defined in Fig. 8. On the (σ, τ) plane, the straight line BC is the bounding curve presented in Eq. (14) which is tangent to the largest Mohr's circle. The length of AO_3 is the radius of the largest Mohr's circle denoting $(\sigma_1 - \sigma_3)/2$. In the right triangle ADO_3, the normal and shear stresses at the point of tangency A are easily obtained as follows:

$$\tau = \frac{\sigma_1 - \sigma_3}{2}\cos\phi \tag{15}$$

$$\sigma = \frac{\sigma_1 + \sigma_3}{2} + \frac{\sigma_1 - \sigma_3}{2}\sin\phi \tag{16}$$

Substituting Eqs. (15) and (16) into Eq. (14), the Mohr–Coulomb criterion is expressed in the space of $(\sigma_1, \sigma_2, \sigma_3)$ as below:

$$\frac{\sigma_1 - \sigma_3}{2} + \frac{\sigma_1 + \sigma_3}{2}\sin\phi = c\cos\phi \tag{17}$$

Recalling Eqs. (6) and (7), the Mohr–Coulomb criterion in Eq. (17) is easily transformed into the space of $(\eta, L, \bar{\sigma})$ in a form of

$$\bar{\sigma}\left(\frac{1}{\sqrt{L^2+3}} + \left(\eta - \frac{L}{3\sqrt{L^2+3}}\right)\sin\phi\right) = c\cos\phi \tag{18}$$

When the Swift's hardening model $\bar{\sigma} = K(\varepsilon_0 + \bar{\varepsilon})^n$ is used, the Mohr–Coulomb criterion is expressed in the space of $(\eta, L, \bar{\varepsilon})$ as below:

$$\bar{\varepsilon}_f = \left(\frac{c\cos\phi}{K\left(\frac{1}{\sqrt{L^2+3}} + \left(\eta - \frac{L}{3\sqrt{L^2+3}}\right)\sin\phi\right)}\right)^{1/n} - \varepsilon_0 \tag{19}$$

From Eq. (19), a cut-off value for the stress triaxiality can be easily obtained by setting the denominator to be zero as below:

$$\frac{1}{\sqrt{L^2+3}} + \left(\eta - \frac{L}{3\sqrt{L^2+3}}\right)\sin\phi = 0 \tag{20}$$

Cut-off values for the stress triaxiality in Eq. (20) are plotted in Fig. 9 with respect to the angle of internal friction in the Mohr–Coulomb criterion. An unrealistically large angle of internal friction

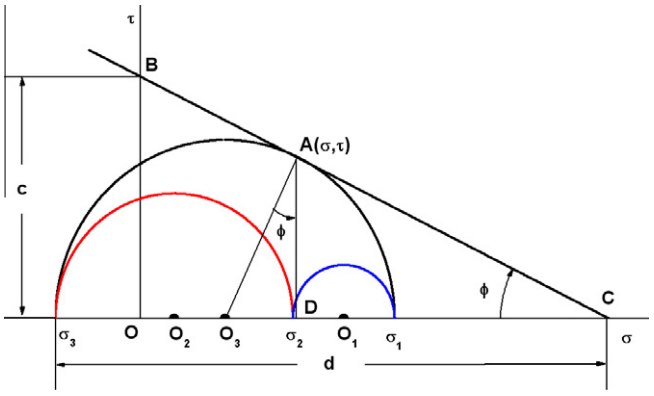

Fig. 8. The Mohr–Coulomb criterion in the Mohr's circles.

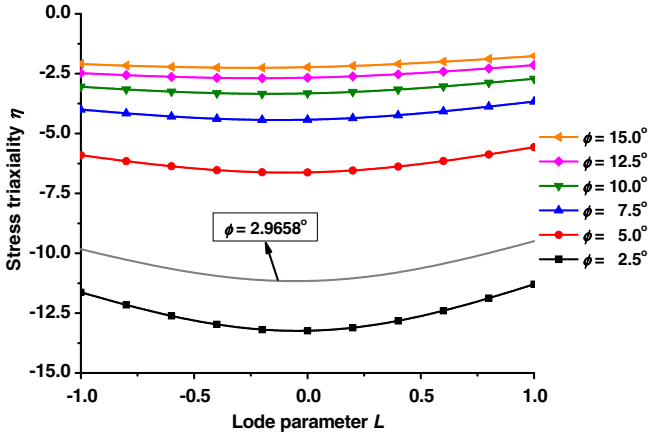

Fig. 9. Cut-off values for the stress triaxiality with respect to the angles of internal friction in the Mohr–Coulomb criterion.

should be selected to obtain a comparatively high cut-off curve for the stress triaxiality. For ductile materials, the angle of internal friction, however, is a very small value which is 2.9658° for 2024-T351 aluminum alloy as presented in Section 5.2. As observed from Fig. 9, the cut-off value for the stress triaxiality is about −10 when the angle of internal friction is 2.9658°. Bao and Wierzbicki (2005) found that the cut-off value for the stress triaxiality is about −1/3 based on analysis of upsetting tests and Bridgman's tests (Bridgman, 1964). The cut-off curve for the stress triaxiality is presented in Fig. 10 when the angle of internal friction is set to an extreme value of 90°. The cut-off values in this extreme case coincide with the line of $\sigma_1 = 0$ in Eq. (8) for which the stress triaxiality increases from −2/3 in the balanced biaxial compression to −1/3 in the uniaxial compression, which coincides with the line of the zero maximum principal stress in Eq. (8).

5. Fracture locus of Al 2024-T351

5.1. Experimental results

Bao (2003) and Bao and Wierzbicki (2004) carried out fifteen different tests on Al 2024-T351 covering a wide range of the stress triaxiality from −0.3 to 1.0, which provide a schematic clue to the effect of the stress triaxiality and the Lode parameter on the

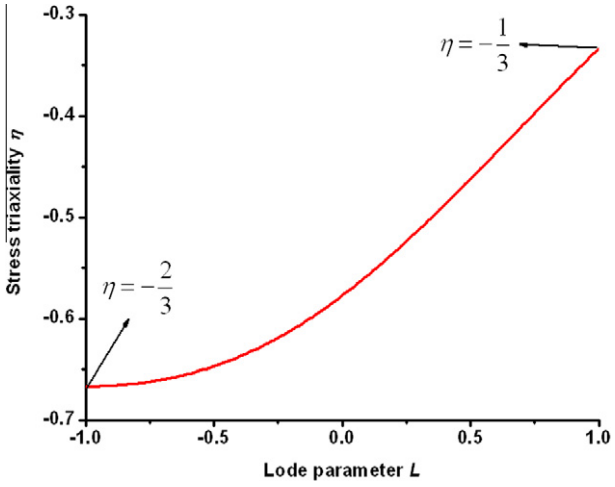

Fig. 10. The cut-off value for the stress triaxiality when $\phi = 90°$ in the Mohr–Coulomb criterion.

equivalent plastic strain to fracture. The equivalent plastic strain to fracture of these tests was presented in Table 1 with the corresponding average stress triaxiality η and the average Lode angle parameter $\bar{\theta}$ by Wierzbicki et al. (2005) and Bai and Wierzbicki (2010) with slight different results.

Since the extended ductile fracture criterion of Eq. (12) is dependent on the stress triaxiality and the Lode parameter, experimental data points in the space of $(\eta, \bar{\theta}, \bar{\varepsilon})$ should be transformed into the space of $(\eta, L, \bar{\varepsilon})$. The principal stresses $(\sigma_1, \sigma_2, \sigma_3)$ were expressed by $(\eta, \bar{\theta}, \bar{\sigma})$ as follows (Bai and Wierzbicki, 2010):

$$\sigma_1 = \sigma_m + s_1 = \sigma_m + \frac{2}{3}\bar{\sigma}\cos\theta = \left(\eta + \frac{2}{3}\cos\theta\right)\bar{\sigma} \tag{21}$$

$$\sigma_2 = \sigma_m + s_2 = \sigma_m + \frac{2}{3}\bar{\sigma}\cos\left(\frac{2}{3}\pi - \theta\right) = \left(\eta + \frac{2}{3}\cos\left(\frac{2}{3}\pi - \theta\right)\right)\bar{\sigma} \tag{22}$$

$$\sigma_3 = \sigma_m + s_3 = \sigma_m + \frac{2}{3}\bar{\sigma}\cos\left(\frac{4}{3}\pi - \theta\right) = \left(\eta + \frac{2}{3}\cos\left(\frac{4}{3}\pi - \theta\right)\right)\bar{\sigma} \tag{23}$$

Using the definition of the Lode parameter of Eq. (5), a one-to-one relation is obtained between the Lode parameter and the Lode angle as below:

$$\tan(\theta) = \frac{\sqrt{3}(L+1)}{3-L} \tag{24}$$

Using the definition of the Lode angle parameter $\bar{\theta} = 1 - (6/\pi)\theta$ (Bai and Wierzbicki, 2010), the relation between the Lode parameter and the Lode angle parameter is derived in a form of

$$\sin\left(\frac{\pi\bar{\theta}}{6}\right) = -\frac{L}{\sqrt{L^2+3}} \tag{25}$$

Since the range of the Lode angle is $0 \leqslant \theta \leqslant \pi/3$, the Lode angle parameter is ranged from -1 to 1 and the Lode parameter is also varied from -1 to 1. When $\theta = 0$, $\bar{\theta} = 1$, $L = -1$, $\sigma_2 = \sigma_3$, the stress state is then a uniaxial tensile stress $(\sigma_1 - \sigma_2, 0, 0)$ together with a hydrostatic stress of σ_2. When $\theta = \pi/6$, $\bar{\theta} = L = 0$, $2\sigma_2 = \sigma_1 + \sigma_3$, the stress state is then a pure shear stress $((\sigma_1 - \sigma_3)/2, 0, (\sigma_3 - \sigma_1)/2)$ together with a hydrostatic stress of $(\sigma_1 + \sigma_3)/2$. When $\theta = \pi/3$, $\bar{\theta} = -1$, $L = 1$, $\sigma_1 = \sigma_2$, the stress state is then a uniaxial compressive stress $(0, 0, \sigma_3 - \sigma_1)$ together with a hydrostatic stress σ_1 or a balanced biaxial tensile stress $(\sigma_1 - \sigma_3, \sigma_1 - \sigma_3, 0)$ together with a hydrostatic stress of σ_3 .

For three-dimensional representation of the fracture locus in the space of $(\eta, L, \bar{\varepsilon})$, the Lode angle θ and the Lode parameter L are then calculated from $\bar{\theta}$ using $\bar{\theta} = 1 - (6/\pi)\theta$ and Eq. (25) representing with the corresponding $\bar{\varepsilon}_f$ and η in Table 1.

5.2. Fracture locus constructed by the Mohr–Coulomb criterion

Two material constants in the Mohr–Coulomb criterion are calibrated by the least square method with all experimental data points presented in Table 1. The fracture locus is constructed and compared with experimental results in Fig. 11. Three branches of plane stress formulated by Eqs. (8)–(10) are presented on the fracture locus: the solid line with hollow squares denotes the zero minimum principal stress; the solid line with hollow diamonds represents the plane stress branch with the zero intermediate principal stress; and the solid line with hollow circles indicates the zero maximum principal stress. Three dashed lines represent the normalized uniaxial tension at $L = -1$, the normalized plane strain of $L = 0$ and the normalized uniaxial compression with $L = 1$, respectively. It should be mentioned that the cut-off value for the stress triaxiality is not presented in Fig. 11. This is because the cut-off value for the stress triaxiality is about -10 for Al 2024-T351 with $\phi = 2.9658^\circ$ as proved in Section 4.

Concerning with the performance of the Mohr–Coulomb criterion, the predicted fracture locus matches to experimental data points near the plane stress state with the test number from 4 to 15 in Table 1. There is great difference in experimental data points of 2 and 3 since ductile fracture for these two experimental points is induced by necking of inter-void ligaments due to the high stress triaxiality while others are caused by shear linking-up of voids.

The fracture locus in the principal strain space is predicted by the Mohr–Coulomb criterion as illustrated in Fig. 12. As the stress triaxiality increases, the material loses ductility since high stress triaxiality accelerates the growth of voids. Besides, the fracture locus is plotted between -2 and 1 for the stress triaxiality. It is observed that the cut-off value for the stress triaxiality is not presented in Fig. 12 since it was too low for the Mohr–Coulomb criterion. At the same stress triaxiality, the fracture strain reaches the maximum value at $L = \pm 1$ while ductile fracture is easily reached in between with low ductility. The minimum fracture strain exists in the normalized plane strain condition at $L = 0$.

5.3. Fracture locus constructed by the new ductile fracture criterion

Material constants in the new ductile fracture criterion are also calculated from the least square method with all experimental data points in Table 1. The new ductile fracture criterion is applied to

Table 1
Experimental data points of Bao (2003) for Al 2024-T351 with the flow stress curve of $\bar{\sigma} = 740\bar{\varepsilon}^{0.15}$ MPa. (After Bai and Wierzbicki, 2010).

Test #	Specimens	$\bar{\varepsilon}_f$	η	$\bar{\theta}$	θ (calculated)	L (calculated)
1	Smooth round bar, tension	0.4687	0.4014	0.9992	4.1888E−4	−0.9990
2	Round large notched bar, tension	0.2830	0.6264	0.9992	4.1888E−4	−0.9990
3	Round small notched bar, tension	0.1665	0.9274	0.9984	8.3776E−4	−0.9980
4	Flat-grooved, tension	0.2100	0.6030	0.0754	0.4841	−0.0684
5	Cylinder ($d_0/h_0 = 0.5$), compression	0.4505	−0.2780	−0.8215	0.9537	0.7946
6	Cylinder ($d_0/h_0 = 0.8$), compression	0.3800	−0.2339	−0.6809	0.8801	0.6451
7	Cylinder ($d_0/h_0 = 1.0$), compression	0.3563	−0.2326	−0.6794	0.8793	0.6435
8	Cylinder ($d_0/h_0 = 1.5$), compression	0.3410	−0.2235	−0.6521	0.8650	0.6155
9	Round notched, compression	0.6217	−0.2476	−0.7141	0.8975	0.6796
10	Pure shear	0.2107	0.0124	0.0355	0.5050	−0.0322
11	Shear tension	0.2613	0.1173	0.3381	0.3466	−0.3099
12	Plate with a circular hole, tension	0.3099	0.3431	0.9661	0.0178	−0.9594
13	Dog-bone specimen, tension	0.4798	0.3570	0.9182	0.0428	−0.9034
14	Pipe, tension	0.3255	0.3557	0.9286	0.0374	−0.9155
15	Solid square bar, tension	0.3551	0.3687	0.9992	4.1888E−4	−0.9990

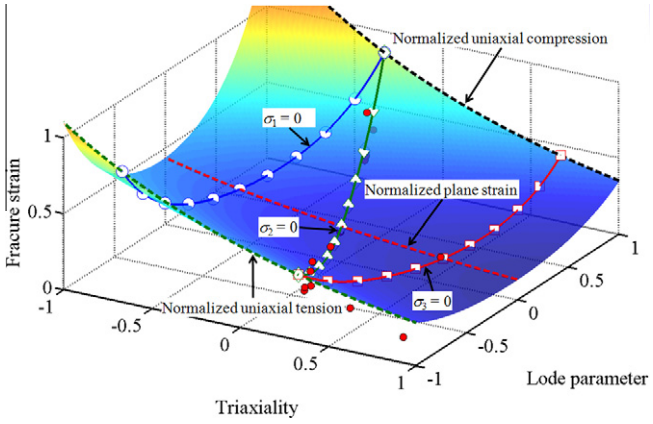

Fig. 11. Fracture locus constructed by the Mohr–Coulomb criterion in the space of $(\eta, L, \bar{\varepsilon})$ for Al 2024-T351. (c = 343.2919 MPa, ϕ = 2.9658°).

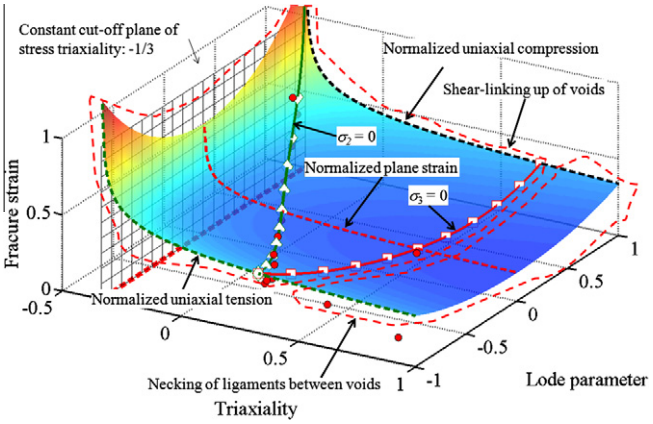

Fig. 13. Fracture locus constructed by the new criterion in the space of $(\eta, L, \bar{\varepsilon})$ for Al 2024-T351. (C_1 = 4.1326, C_2 = 0.2235, C_3 = 0.3896).

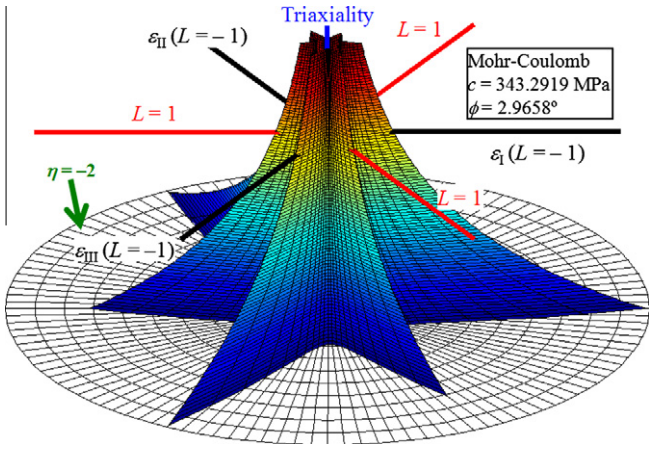

Fig. 12. Fracture locus constructed by the Mohr–Coulomb criterion in the principal strain space for Al 2024-T351.

construct the fracture locus of Al 2024-T351 as presented in Fig. 13. The fracture locus is observed to be symmetric with respect to $L = 0$, which can be proved in Eq. (12). It makes sense for the shear linking-up of voids caused by the maximum shear stress which is also a symmetric function of the Lode Parameter as shown in Eq. (11). Moreover, the fracture locus of the new ductile fracture criterion is a monotonic function of the stress triaxiality, which means that materials lose ductility at the high stress triaxiality. A cut-off plane for the stress triaxiality exists at $\eta = -1/3$ which is intentionally coupled in the new ductile fracture criterion. Two branches of plane stress, $\sigma_2 = 0$ and $\sigma_3 = 0$, can be easily obtained by setting Eqs. (9) and (10) to be zero as presented in Figs. 11 and 13. One additional branch of plane stress, denoted as $\sigma_1 = 0$, is not presented in Fig. 13 since the stress triaxiality of this branch ranges from $-2/3$ in the normalized uniaxial tension ($L = -1$) to $-1/3$ in the normalized uniaxial compression ($L = 1$) which is below the cut-off value of $-1/3$ assumed in the new ductile fracture criterion. Three special lines are represented in Fig. 13 to denote the normalized uniaxial tension ($L = -1$), the normalized pure shear or plane strain ($L = 0$) and the normalized uniaxial compression ($L = 1$).

Compared with experimental results, the fracture locus constructed by the new criterion is close to the experimental data points except two types of experiments with the test number of 2 and 3 in Table 1. This is due to the fact that coalescence of voids in the uniaxial tension of notched round bars is caused by necking of ligaments between voids in the center of notched specimens due to the high stress triaxiality. The development of the new ductile fracture criterion, however, is based on the assumption of the shear linking-up of voids (Lou et al., 2012). Consequently, the application of the new ductile fracture is limited to the stress state where ductile fracture is induced by the shear linking-up of voids. Even though the bounding line between two coalescence mechanisms still is not clear, the new ductile fracture criterion can be successfully applied to predict ductile fracture of sheet metals and bulk metals in low and negative stress triaxiality as observed in Fig. 13.

The new fracture locus is also illustrated in Fig. 14 in the principal strain space. Increasing stress triaxiality is observed to reduce the ductility of the material due to the accelerated void growth in high stress triaxiality. Moreover, the cut-off value for the stress triaxiality is plotted to be constant at $\eta = -1/3$. At constant stress triaxiality, the fracture strain reaches the maximum value at $L = \pm 1$ while ductile fracture is easily reached in between with low ductility. The minimum fracture strain exists in the normalized plane strain condition at $L = 0$. This Lode dependence of the proposed fracture model is similar with that of the Mohr–Coulomb criterion in Fig. 12. The difference is that the predicted fracture strain in the normalized uniaxial tension at $L = -1$ is identical with that in the normalized uniaxial compression at $L = 1$ for the proposed fracture criterion while the Mohr–Coulomb criterion predicts different ductility in these two loading conditions.

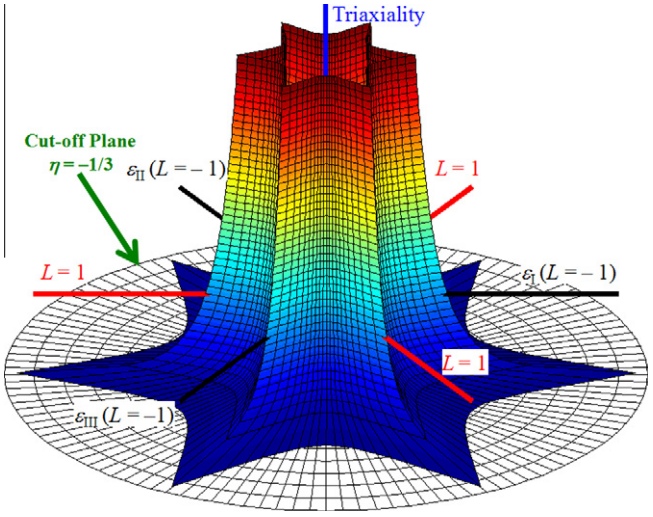

Fig. 14. Fracture locus constructed by the new criterion in the principal strain space for Al 2024-T351.

Compared to the fracture locus constructed by the Mohr–Coulomb criterion in Figs. 11 and 12, there are two obvious merits of the new fracture locus. The first merit is that the proposed fracture locus couples a reasonable cut-off value of $-1/3$ for the stress triaxiality according to Bao and Wierzbicki (2005) even though there are limitations of their results such as omission of the effect for the microstructures, temperature and Lode parameter. The importance of a cut-off value has already been confirmed in high velocity impact simulation (Teng and Wierzbicki, 2006). The second merit is that a symmetric fracture locus with respect to $L = 0$ is constructed by the new ductile fracture criterion. This is sound for shear linking-up of voids along the direction of the maximum shear stress which is also a symmetric function of the Lode parameter.

6. Conclusions

A newly proposed ductile fracture criterion for sheet metals is extended to a general three dimensional stress state with dependence of the stress triaxiality and the Lode parameter to estimate the equivalent plastic strain to fracture for bulk metals. The mechanism for the Lode parameter dependence of ductile fracture is correlated to the effect of the maximum shear stress on the coalescence of voids to construct the extended form of the new ductile fracture criterion. The extended ductile fracture criterion is successfully applied to construct the fracture locus of Al 2024-T351 with high accuracy for ductile fracture induced by shear linking-up of voids. Moreover, the technique of the Mohr's circles is properly utilized to transform the Mohr–Coulomb criterion to the space of $(\eta, L, \bar{\varepsilon})$ without any difficulties. The transformed Mohr–Coulomb criterion is utilized to predict the equivalent plastic strain to fracture of Al 2024-T351. The fracture loci constructed are compared between the Mohr–Coulomb criterion and the new criterion. Comparison reveals that the new criterion has a favorable merit in that a reasonable cut-off value for the stress triaxiality is coupled for ductile fracture of metals.

References

Aretz, H., 2011. Private communication.

Argon, A.S., Im, J., Safoglu, R., 1975. Cavity formation from inclusions in ductile fracture. Metall. Trans. 6A, 825–837.

Bai, Y., Wierzbicki, T., 2010. Application of extended Mohr–Coulomb criterion to ductile fracture. Int. J. Fract. 161, 1–20.

Bao, Y.B., 2003. Prediction of ductile crack formation in uncracked bodies. Ph.D. Thesis, Massachusetts Institute of Technology.

Bao, Y.B., Wierzbicki, T., 2004. On fracture locus in the equivalent strain and stress triaxiality space. Int. J. Mech. Sci. 46, 81–98.

Bao, Y.B., Wierzbicki, T., 2005. On the cut-off value of negative triaxiality for fracture. Eng. Fract. Mech. 72, 1049–1069.

Bridgman, P.W., 1964. Studies in Large Plastic Flow and Fracture. Harvard University Press, Cambridge, MA.

Brozzo, P., DeLuca, B., Rendina, R., 1972. A new method for the prediction of the formability limits of metal sheets. In: Proceedings of the 7th Biennial Conference of IDDRG on Sheet Metal Forming and Formability.

Chen, X.M., Shi, M.F., Shih, H.-C., Luo, M., Wierzbicki, T., 2010. AHSS shear fracture predictions based on a recently developed fracture criterion. SAE Int. J. Mater. Manuf. 3, 723–731.

Clift, S.E., Hartley, P., Sturgess, C.E.N., Rowe, G.W., 1990. Fracture prediction in plastic deformation processes. Int. J. Mech. Sci. 32, 1–17.

Cockcroft, M.G., Latham, D.J., 1968. Ductility and the workability of metals. J. Inst. Metals 96, 33–39.

Dunand, M., Mohr, D., 2011. On the predictive capabilities of the shear modified Gurson and the modified Mohr–Coulomb fracture models over a wide range of stress triaxialities and Lode angles. J. Mech. Phys. Solids 59, 1374–1394.

Fung, Y.C., Tong, P., 2001. Classical and computational solid mechanics. In: Elastic and Plastic Behavior of Materials. World Scientific Publication, Singapore.

Goods, S.H., Brown, L.M., 1979. The nucleation of cavities by plastic deformation. Acta Metall. 27, 1–15.

Goodwin, G.M., 1968. Application of strain analysis to sheet metal forming problems in the press shop. SAE Technical Paper No. 680093.

Gurson, A.L., 1977. Continuum theory of ductile rupture by void nucleation and growth. Part I: yield criteria and flow rules for porous ductile media. ASME J. Eng. Mater. Technol. 99, 2–15.

Halford, G.R., Morrow, J., 1962. On low-cycle fatigue in torsion. In: Proceedings of ASTM, vol. 62, pp. 695–707.

Hill, R., 1952. On discontinuous plastic states, with special reference to localized necking in thin sheets. J. Mech. Phys. Solids 1, 19–30.

Hora, P., Tong, L., Reissner, J., 1996. A prediction method for ductile sheet metal failure in FE-simulation. In: Proceedings of the Numisheet'96 Conference, Dearborn, Michigan, USA, pp. 252–256.

Kao, A.S., Kuhn, H.A., Richmond, O., Spitzig, W.A., 1990. Tensile fracture and fractographic analysis of 1045 spheroidized steel under hydrostatic pressure. J. Mater. Res. 5, 83–91.

Keeler, S.P., Backofen, W.A., 1963. Plastic instability and fracture in sheets stretched over rigid punches. Trans. ASM 56, 25–48.

Khan, A.S., Liu, H.W., 2012. A new approach for ductile fracture prediction on Al 2024-T351. Int. J. Plasticity 35, 1–12.

Ko, Y.K., Lee, J.S., Huh, H., Kim, H.K., Park, S.-H., 2007. Prediction of fracture in hub-hole expanding process using a new ductile fracture criterion. J. Mater. Process. Technol. 187 (188), 358–362.

LeRoy, G., Embury, J., Edwards, G., Ashby, M.F., 1981. A model of ductile fracture based on the nucleation and growth of voids. Acta Metall. 29, 1509–1522.

Li, H., Fu, M.W., Lu, J., Yang, H., 2009. Ductile fracture: experiments and computations. Int. J. Plasticity 27, 147–180.

Li, Y.N., Luo, M., Gerlach, J., Wierzbicki, T., 2010. Prediction of shear-induced fracture in sheet metal forming. J. Mater. Process. Technol. 210, 1858–1869.

Lode, W., 1926. Versuche über den Einfluss der mittleren Hauptspannung auf das Fliessen der Metalle Eisen, Kupfer, und Nickel. Z. Phys. 36, 913–939.

Lou, Y.S., Huh, H., Lim, S., Pack, K., 2012. New ductile fracture criterion for prediction of fracture forming limit diagrams of sheet metals. Int. J. Solids Struct. 49, 3605–3615.

Luo, M., Chen, X.M., Shi, M.F., Shih, H.-C., 2010. Numerical analysis of AHSS fracture in a stretch-bending test. In: AIP Conference Proceedings of the 10th International Conference on NUMIFORM 1252, pp. 455–463.

Marciniak, Z., Kuczynski, K., 1967. Limit strains in the processes of stretch-forming sheet metal. Int. J. Mech. Sci. 9, 609–620.

McClintock, F.A., 1968. A criterion for ductile fracture by the growth of holes. ASME J. Appl. Mech. 35, 363–371.

Nielsen, K.L., Tvergaard, V., 2010. Ductile shear failure or plug failure of spot welds modeled by modified Gurson model. Eng. Fract. Mech. 77, 1031–1047.

Oh, S.I., Chen, C.C., Kobayashi, S., 1979. Ductile fracture in axisymmetric extrusion and drawing: Part 2, workability in extrusion and drawing. ASME J. Eng. Ind. 101, 36–44.

Oyane, M., Sato, T., Okimoto, K., Shima, S., 1980. Criteria for ductile fracture and their applications. J. Mech. Work. Technol. 4, 65–81.

Rice, J.R., Tracey, D.M., 1969. On the ductile enlargement of voids in triaxial stress fields. J. Mech. Phys. Solids 17, 201–217.

Stören, S., Rice, J.R., 1975. Localized necking in thin sheets. J. Mech. Phys. Solids 23, 421–441.

Swift, H.W., 1952. Plastic instability under plane stress. J. Mech. Phys. Solids 1, 1–19.

Teng, X., Wierzbicki, T., 2006. Evaluation of six fracture models in high velocity perforation. Eng. Fract. Mech. 73, 1653–1678.

Tvergaard, V., Needleman, A., 1984. Analysis of the cup–cone fracture in a round tensile bar. Acta Metall. 32, 157–169.

Weck, A., Wilkinson, D., 2008. Experimental investigation of void coalescence in metallic sheets containing laser drilled holes. Acta Mater. 56, 1774–1784.

Wierzbicki, T., Bao, Y.B., Lee, Y.-W., Bai, Y.L., 2005. Calibration and evaluation of seven fracture models. Int. J. Mech. Sci. 47, 719–743.

Xue, L., 2007. Damage accumulation and fracture initiation in uncracked ductile solids subject to triaxial loading. Int. J. Solids Struct. 44, 5163–5181.

Xue, L., Wierzbicki, T., 2008. Ductile fracture initiation and propagation modeling using damage plasticity theory. Eng. Fract. Mech. 75, 3276–3293.

Xue, L., 2008. Constitutive modeling of void shearing effect in ductile fracture of porous materials. Eng. Fract. Mech. 75, 3343–3366.

Zhu, X., Weinmann, K., Chandra, A., 2001. A unified bifurcation analysis of sheet metal forming limits. ASME J. Eng. Mater. Technol. 123, 329–333.